Effects of silibinin-loaded thermosensitive liposome-microbubble complex on inhibiting rabbit liver VX2 tumors in sub-hyperthermia fields

LU HAN[1*], KAI GUO[2*], FEN GU[1*], YUN-FEI ZHANG[3], KE LI[1], XI-XI MU[4], HAI-JING LIU[1], XIAO-DONG ZHOU[1] and WEN LUO[1]

[1]Department of Ultrasound, Xijing Hospital, Fourth Military Medical University, Xi'an, Shaanxi 710032; Departments of [2]Thoracic Surgery and [3]Orthopedics, Tangdu Hospital, Fourth Military Medical University, Xi'an, Shaanxi 710038; [4]Department of General Surgery, Xijing Hospital, Fourth Military Medical University, Xi'an, Shaanxi 710032, P.R. China

Received February 12, 2017; Accepted September 1, 2017

DOI: 10.3892/etm.2017.5566

Abstract. In the present study, the effects of silibinin-loaded thermosensitive liposome-microbubble complex (STLMC) on rabbit liver VX2 tumors in sub-hyperthermia fields were investigated using two-dimensional ultrasonography (2D US), contrast-enhanced US (CEUS), hematoxylin and eosin (H&E) staining, immunohistochemistry and ultrastructure observation. 50 rabbits with VX2 liver tumors were divided into five groups: Sub-hyperthermia microwave ablation group (SHM), STLMC injection group (STLMC), SHM ablation plus STLMC injection group (SHM + STLMC), microbubble injection group and blank control group without any treatment. Rabbits in each group were examined using 2D US and CEUS in order to evaluate the tumor volume and diameter before treatment and at day 7 and 21 after treatment. Morphology, expression of CD163 and CD206, and ultrastructure of the tumors were assessed. The average post-treatment volume of tumors in group SHM + STLMC was 1.17±0.88 cm^3 at day 7 and 2.15±0.96 cm^3 at day 21, which was significantly decreased compared with all other groups ($P<0.05$). H&E staining indicated that the number of disordered macrophages in the SHM + STLMC group significantly increased compared with the other groups ($P<0.05$). Immunohistochemical results demonstrated that in the SHM + STLMC, the expression of CD163 and CD206 significantly decreased compared with all other groups ($P<0.05$). These results suggested that STLMC has a potential function in preventing tumor growth, which may be due to its inhibitory effect on tumor-associated macrophages in the tumor microenvironment.

Correspondence to: Professor Wen Luo or Professor Xiao-Dong Zhou, Department of Ultrasound, Xijing Hospital, Fourth Military Medical University, 127 Changle Road, Xi'an, Shaanxi 710032, P.R. China
E-mail: lwdd1234@fmmu.edu.cn
E-mail: zhouxd@fmmu.edu.cn

*Contributed equally

Key words: silibinin-loaded thermosensitive liposome-microbubble complex, VX2 tumors, sub-hyperthermia fields, macrophages, microwave ablation

Introduction

Primary liver cancer is the sixth most commonly occurring cancer type in the world and the second largest contributor to cases of cancer-related mortality (1). In recent decades, thermal ablation technology in the treatment of liver tumors has developed rapidly. By increasing the temperature above 50-60˚C on the treatment region for a few sec, ablation treatment reliably necrotizes viable tissues (2). However, therapeutic effects of ablation treatment on hepatocellular carcinoma (HCC) are limited by multiple factors. For example, because of the 'heat-sink effect', it is difficult to achieve high temperatures in areas located next to the large vessels (3). Therapeutic ranges of ablation were also affected by the different tumor locations. Therefore, the heterogeneity of temperature distribution results in sub-hyperthermia fields (41-50˚C), which may be the reason for residual tumors after thermal ablation treatment (4,5).

The tumor inflammatory microenvironment, which consists of stromal cells, inflammatory cytokines and extracellular matrix proteins, serves critical functions in liver fibrosis, hepatocarcinogenesis, epithelial-mesenchymal transition (EMT), tumor invasion and metastasis (6,7). Among the stromal cells within the inflammatory microenvironment of the HCC, tumor-associated macrophages (TAMs) are critical components of tumor-related inflammation (8). Previous studies have demonstrated that TAMs are primarily polarized towards alternatively activated macrophages (9,10) with the markers of CD163, CD301 and CD206 (11,12), which are thought to be closely associated with the angiogenesis, immunosuppression and activation of tumor cells (6).

Silymarin and its major constituent, silibinin, are extracted from the medicinal plant *Silybum marianum* (milk thistle) (13). Previous studies reported that silibinin can inhibit multiple cancer cell signaling pathways, including inhibition of growth and angiogenesis, and regulation of EMT (13-15). However,

its poor permeability and targeting has limited its biological effects (16,17). In a previous study by the current group, a new drug carrier was designed, combining thermosensitive liposome with ultrasound contrast agent microbubbles. The silibinin was loaded within the thermosensitive liposome, of which the entrapment efficacy could reach 71.0±8.3% (18). Destruction of microbubbles by high-intensity ultrasound opened the vascular endothelial barrier (19), and the thermosensitive liposome was able to be released in sub-hyperthermia fields. At the temperature of 40-42˚C, the average release percentage was >50% (18).

In order to investigate the effects of silibinin-loaded thermosensitive liposome-microbubble complex (STLMC) *in vivo*, in the present study, low-power microwaves were used to simulate sub-hyperthermia fields, and STLMC was used to treat rabbit liver VX2 tumors. The effects on growth of tumors and histopathology were observed, and the potential association with TAMs was evaluated.

Materials and methods

Animals. The experiments were approved by the Institutional Animal Care and Use Ethics Committee of the Fourth Military Medical University (Xi'an, China). A total of 60 healthy adult male New Zealand white rabbits (age, 12 weeks; weight, 2.75±0.25 kg) were purchased from the Laboratory Animal Center of Fourth Military Medical University. One tumor-bearing adult male New Zealand white rabbit (age, 12 weeks; weight, 2.5 kg) with VX2 tumor in the thigh was purchased from the Lianyungang Second People's Hospital (Lianyungang, China). The rabbits were maintained under a 12-h light/dark cycle under constant temperature of 20±5˚C and 60-65% humidity, and received a standard laboratory diet and drinking water.

Implantation process of VX2 liver tumors. The VX2 tumor tissue in the thigh of the tumor-bearing rabbit was resected and cut into pieces ~1 mm^3 in size under sterile conditions. The 50 recipient animals were anesthetized by ear vein injection with 3% pentobarbital solution (30 mg/kg), and their abdomens were shaved and prepared with povidone iodine. Guided by a conventional ultrasound image, a 16-gauge puncture needle carrying 2-3 fragments of tumor tissue and one small piece of gelatin foam was percutaneously inserted into the hepatic parenchyma, and then the tumor tissues were injected and implanted (20).

Establishment of sub-hyperthermia field. A microwave electrode (ECO-100C; ECO Medical Instrument Co., Ltd., Nanjing, China) was employed for ablation on the liver of 10 rabbits. With guidance of ultrasound, the microwave needle was inserted into normal rabbit liver tissue. In order to imitate sub-hyperthermia field at 40-42˚C, three different output powers of 20, 25 and 30 W were set for ablation. The procedure was scheduled as follows: Ablation was maintained for 1 min, then the power was turned to 0 W for 1 min, then repeated for 10 min in total. A thermocouple needle (HYP3-16-1-1/2-K-G-48-SMPW-M; Omega Bio-Tek, Inc., Norcross, GA, USA) was placed at three different distances from the microwave needle (5, 10 or 15 mm), and connected with a thermometer (HH11B; Omega Bio-Tek, Inc.), which reported the temperature data digitally. The temperature, microwave output power and duration were recorded and used to determine microwave output power and duration for achieving a 40-42˚C thermal field.

Intervention on VX2 tumors. Fourteen days after implantation of VX2 tumors, the recipient animals were assigned to five groups (10 animals per group): Sub-hyperthermia microwave ablation group (SHM), STLMC injection group (STLMC), SHM ablation plus STLMC injection group (SHM + STLMC), microbubble group (MB) and blank control group (BL). Rabbits in each group were fasted for 24 h before treatments, then anesthetized by ear vein injection with 3% pentobarbital solution (30 mg/kg).

In the SHM group, under ultrasound guidance, the microwave needle was inserted into the tumor percutaneously, in order to establish the sub-hyperthermia field according to the aforementioned parameters of output power and ablation time.

In the STLMC group, 8 ml STLMC solution (containing 8 μg/ml silibinin, which was purchased from the National Institutes for food and drug control, Beijing, China; 110856-201506), supplied by Department of Ultrasound, Xijing Hospital, Fourth Military Medical University) was continuously pumped via the ear vein for 10 min (18), then 2 ml 0.9% normal saline solution was injected. Simultaneously, an ultrasound probe (L522; Esaote SpA, Florence, Italy) was used to scan the tumor region in flash mode with 100% power, in order to destroy the microbubbles.

In the SHM + STLMC group, 10 rabbits with VX2 tumors in this group were treated according to the two aforementioned methods.

In the MB group, 8 ml SonoVue solution (Bracco SpA, Milan, Italy) was injected by a pump via the ear vein. The ultrasound probe was used to destroy the microbubbles in flash mode with 100% power.

The animals in the BL group received no treatment. In each group, 5 animals were sacrificed at day 7 and 21 after treatment, respectively.

2D ultrasonography (US). Before and after treatment, 2D US was employed to determine the position of tumors and measure the length (L), width (W), and depth (D) of VX2 tumors using a 7.5-MHz linear probe (L522) and Mylab90 ultrasound imaging system (Esaote SpA). The tumor volume (V) was calculated with the formula: $V=(\pi/6)$ L x W x D.

Contrast-enhanced US (CEUS). Before and after treatment, animals were injected with 0.2 ml SonoVue and 2 ml 0.9% saline via ear vein for enhanced images on MyLab 90 system (Esaote SpA) with L522 probe. The maximum diameter of tumor was measured. The contrast enhanced cine loops were observed and stored in the equipment.

The blood flow distribution of the tumors in CEUS was evaluated and classified with four grades: 0, non-perfusion; 1, dot-like perfusion; 2, strip-like perfusion; 3, island perfusion.

Hematoxylin and eosin staining (H&E). Rabbits were administered with 3% pentobarbital solution (30 mg/kg) and euthanized using air embolization. VX2 tumors were excised, fixed in a 10% neutral formalin solution for 24 h under constant temperature of 22±2˚C and embedded in paraffin. Tumor sections (5 μm) were prepared for hematoxylin and eosin staining (with

hematoxylin for 10 min and eosin for 1 min at room temperature). The sections were observed under a light microscope by an experienced pathologist. In each animal, five sections with 10 random areas each were examined at x200 magnification.

Immunohistochemistry. The excised VX2 tumor tissues were fixed in 4% (w/v) paraformaldehyde for 24 h at room temperature, embedded in paraffin and sliced into 4 μm sections. Tissue sections were deparaffinized in xylene and hydrated gradually through graded alcohol and processed with Tris/EDTA buffer solution (pH 9.0) and high pressure cooker, >120˚C for 3 min. Endogenous peroxidase activity was blocked with 3% hydrogen peroxide for 15 min. The slides were then blocked with 10% goat serum (AR0009, Boster Biological Technology Co., Ltd., Wuhan, China) for 2 h at room temperature, and primary antibodies of CD206 (1:25, ab117644; Abcam, Cambridge, UK) and CD163 (1:50, ab111250; Abcam) were applied overnight at 4˚C. The biotin-labeled secondary antibody (KIT-7710; Maixin Biotech Co., Ltd., Fuzhou, China) was applied for 1 h at room temperature. The sections were stained at room temperature with diaminobenzidine tetrahydrochloride (Maixin Biotech Co., Ltd.) for 50 sec and finally counterstained with hematoxylin for 8 min. Sections stained in the absence of primary antibodies were used as negative controls.

Five slides from each animal were examined under light microscopy. The proportion of positive cells was estimated among the total number of the cells by observing five random fields at x400 magnification.

Transmission electron microscope (TEM). The previously embedded tumor tissues were divided into 1 mm^3 pieces and fixed with 2.5% glutaraldehyde and 4% paraformaldehyde for 2 h at 4˚C. Then, using standard procedures, ultra-thin (50 nm) sections were prepared and stained with uranyl acetate (for 30 min at 35˚C) and lead citrate (for 10 min at 20˚C), and changes in the macrophages were observed using TEM (Tecnai Spirit, Hillsboro, Oregon State, USA). In each group, 100 fields of vision were randomly selected to observe the ultrastructure (magnification x6,000).

Statistical analysis. SPSS software (version 22.0, IBM Corp., Armonk, NY, USA) was used to analyze the data. Data were presented as the mean ± standard deviation. One-way analysis of variance and the least significant difference test were used to analyze the differences among multiple groups. Differences between two groups were assessed with Student's t-test or Chi-squared test. P<0.05 was considered to indicate a statistically significant difference.

Results

Establishment of sub-hyperthermia field. Fig. 1 indicates the thermometry results of using different microwave output powers and distances. Via microwave ablation with 20 W output power for 1 min ablation with 1 min interval, the simulative sub-hyperthermia field (40-42˚C) was established in the areas, with 10 mm distance to the microwave needle.

2D US of rabbit liver VX2 tumor. The tumor volumes of the five groups are shown in Fig. 2. Before ablation, there were no significant differences in tumor volume between groups (P>0.05). However, the volume of tumors in the SHM + STLMC group on days 7 and 21 after surgery were 1.17±0.88 and 2.15±0.96 cm^3, respectively, which was significantly lower compared with the other four groups (P<0.05) at the same time points.

CEUS of rabbit liver VX2 tumor. CEUS indicated distinct peripheral enhancement of VX2 tumors at the early arterial phase and then quick washout of contrast agents. The maximum tumor diameters in the five groups measured by CEUS are

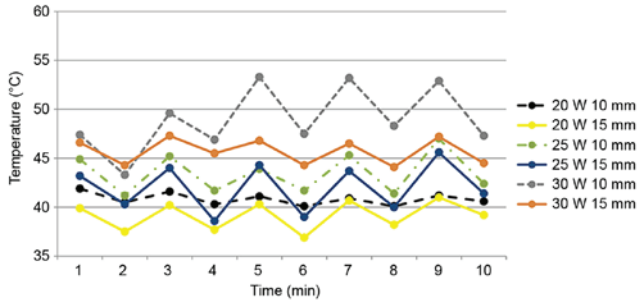

Figure 1. Thermal field distributions under different parameters.

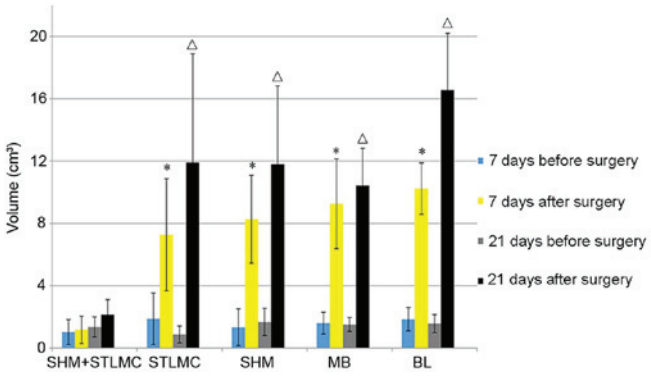

Figure 2. VX2 tumor volumes in each group, observed using 2D ultrasonography. *P<0.05 vs. 7 days after surgery in the SHM + STLMC group; ΔP<0.05 vs. 21 days after surgery in the SHM + STLMC group. SHM, sub-hyperthermia microwave ablation; STLMC, silibinin-loaded thermosensitive liposome-microbubble complex; MB, microbubble injection; BL, blank control.

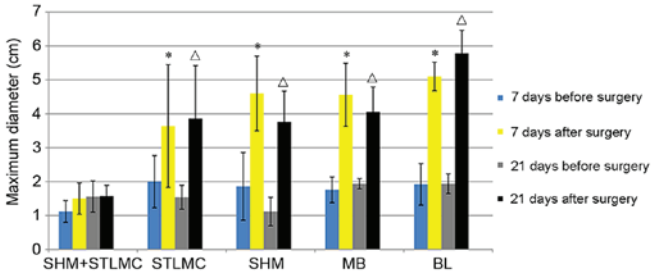

Figure 3. VX2 tumor maximum diameters, observed using contrast-enhanced ultrasonography. *P<0.05 vs. 7 days after surgery in the SHM + STLMC group; ΔP<0.05 vs. 21 days after surgery in the SHM + STLMC group. SHM, sub-hyperthermia microwave ablation; STLMC, silibinin-loaded thermosensitive liposome-microbubble complex; MB, microbubble injection; BL, blank control.

Table I. Blood flow distribution of tumors measured by contrast-enhanced ultrasonography.

	Day 7				Day 21			
Group	Grade 0	Grade 1	Grade 2	Grade 3	Grade 0	Grade 1	Grade 2	Grade 3
SHM + STLMC	4	1	0	0	4	1	0	0
SHM[a,b]	0	1	2	2	0	2	1	2
STLMC[a,b]	0	2	1	2	0	0	2	3
MB[a,b]	0	0	1	4	0	0	0	5
BL[a,b]	0	0	0	5	0	0	0	5

Results are expressed as the number of tumors. P-values were calculated using the χ-squared test. [a]P<0.05 vs. day 7 in the SHM + STLMC group, [b]P<0.05 vs. day 21 in the SHM + STLMC group. SHM, sub-hyperthermia microwave ablation; STLMC, silibinin-loaded thermosensitive liposome-microbubble complex; MB, microbubble injection; BL, blank control.

shown in Fig. 3. Before ablation, there were no significant differences between groups (P>0.05). The maximum diameter of the tumors on days 7 and 21 after surgery in the SHM + STLMC group were significantly smaller compared with the other groups (P<0.05) at the same time points. No significant differences in the maximum diameter were observed between days 7 and 21 in the SHM + STLMC group (P>0.05).

The typical CEUS images of each group on day 7 after the treatment are shown in Fig. 4. Table I presents the blood flow distribution of tumors measured by CEUS. Statistical analysis indicated that postoperative blood flow on days 7 and 21 was significantly reduced in the SHM + STLMC group compared with other groups (P<0.05).

TEM of rabbit liver VX2 tumor. At day 7 after treatment, macrophages with obvious tumefaction of mitochondria, blurred and indistinct mitochondrial cristae, a decreasing number of lysosomes and increased heterochromatin within the cell nucleus were observed in the SHM + STLMC group (Fig. 5A). At day 21 after treatment, changes in macrophages were observed in the SHM + STLMC group, including the enlargement of the cell nucleus, disproportionality of endochylema, margination of nuclear chromatin, expansion of endoplasmic reticulum and decreased lysosomes (Fig. 5B). Compared with other groups, the number of damaged macrophages significantly increased in the SHM + STLMC group (P<0.05; Table II). This damage was significantly increased on day 21 compared with day 7 (P<0.05).

By using TEM, other inflammatory cells were observed in the SHM + STLMC group at day 21. Plasmacytes with an increased block of heterochromatin distributed across one side of the nuclear membrane, blurred and indistinct mitochondrial cristae and augmented volume were observed. Morphological abnormalities were observed in lymphocytes, with decreased ribosomes and dilated rough endoplasmic reticulum. In monocytes, enlarged nuclei and disordered nucleus-cytoplasm ratios were widespread phenomenon. Decreased organelles, including mitochondria, ribosomes and phagocytic vesicles, could be observed in the monocytes, as well as the emergence of apoptotic bodies and nuclear chromatin clumping.

However, the morphology of macrophages was basically normal in the STLMC group, and the mitochondria of macrophages were mildly swollen in SHM group (Fig. 5C). The morphology and structure of macrophages and other inflammatory cells were basically normal in the MB and BL groups.

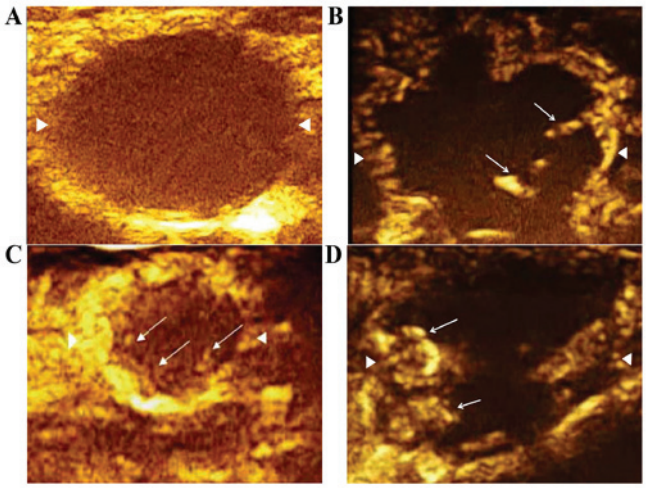

Figure 4. Contrast-enhanced ultrasonography images of each group at day 7 after treatment. The tumor boundary is indicated with white triangles. (A) Grade 0 (non-perfusion) surrounding the ablated area in the SHM + STLMC group. (B) Grade 1 (dot-like perfusion) surrounding the ablated area in the SHM group, indicated by white arrows. (C) Grade 2 (strip-like perfusion) in the tumor center in the STLMC group, indicated by white arrows. (D) Grade 3 (island perfusion) surrounding the ablated area in the MB group, indicated by white arrows. SHM, sub-hyperthermia microwave ablation; STLMC, silibinin-loaded thermosensitive liposome-microbubble complex; MB, microbubble injection.

Histopathology of rabbit liver VX2 tumor. A large number of macrophages with larger volume and irregular shape were observed, with hyperchromatism in the SHM + STLMC group. Macrophages with multiple nuclei were detected around the tumor tissues and necrotic areas in the SHM + STLMC group (Fig. 5D and E). In the STLMC and SHM (Fig. 5F) groups, a small number of abnormal macrophages were observed. In the MB and BL groups, the general morphology of cells was normal. The number of disordered macrophages in the SHM + STLMC group at days 7 and 21 were 16.86±5.33 and 19.12±4.12/high power field (HPF), respectively, which was a significant increase compared with the other groups (P<0.05; Table III).

Table II. Number of damaged macrophages observed under transmission electron microscopy.

	Day 7					Day 21				
Group	SHM + STLMC	SHM	STLMC	MB	BL	SHM + STLMC	SHM	STLMC	MB	BL
n/HPF	0.75±0.67	0.24±0.47[a]	0.30±0.58[a]	0.55±0.22[a]	0.04±0.20[a]	1.09±0.90[c]	0.38±0.60[b]	0.40±0.57[b]	0.11±0.35[b]	0.09±0.28[b]

Data are presented as the mean ± standard deviation. Comparisons among groups were analyzed using one-way analysis of variance. Followed by the least significant difference test. Comparisons between time points were analyzed using Student's t-test. [a]P<0.05 vs. day 7 SHM + STLMC; [b]P<0.05 vs. day 21 SHM + STLMC; [c]P<0.05 vs. day 7 SHM + STLMC. SHM, sub-hyperthermia microwave ablation; STLMC, silibinin-loaded thermosensitive liposome-microbubble complex; MB, microbubble injection; BL, blank control; HPF, high power field.

Figure 5. Histopathology and ultrastructure changes of the macrophages in VX2 tumors. (A) TEM image of the SHM + STLMC group at day 7 after treatment (scale bar=1 μm; a magnification x6,000 was used for counting and a magnification of x15,000 was used for observing and presenting the ultrastructure). Increased nucleus size, chromatin margination (black arrow), cell vacuolation (white arrow) and a decreased number of organelles were observed. (B) TEM image of the SHM + STLMC group at day 21 after treatment (scale bar=1 μm; a magnification x6,000 was used for counting and a magnification of x15,000 was used for observing and presenting the ultrastructure). Chromatin margination and increased heterochromatin (black arrow), damaged organelle (white arrow) were observed. (C) TEM image of the SHM group at day 7 after treatment (scale bar=1 μm; a magnification x6,000 was used for counting and a magnification of x15,000 was used for observing and presenting the ultrastructure). Cell vacuolation (white arrow) was observed. (D) H&E staining of the SHM + STLMC group at day 7 after treatment (scale bar=20 μm; a magnification of x200 was used for counting and a magnification of x400 was used to observe the macrophages). Damaged macrophages were observed in the ablated area (black arrow). (E) H&E staining of the SHM + STLMC group at day 21 after treatment (scale bar=20 μm; a magnification of x200 was used for counting and a magnification of x400 was used to observe the macrophages). Damaged macrophages were observed in the ablated area (black arrow). (F) H&E staining of the SHM group at day 21 after treatment (scale bar=20 μm; a magnification of x200 was used for counting and a magnification of x400 was used to observe the macrophages). Damaged macrophages were observed in the ablated area (black arrow). TEM, transmission electron microscopy; H&E, hematoxylin and eosin; SHM, sub-hyperthermia microwave ablation; STLMC, silibinin-loaded thermosensitive liposome-microbubble complex.

Immunohistochemical study. Macrophages were examined using immunohistochemical detection of CD163 and CD206. A small number of cells were positively stained for these macrophage markers in the SHM + STLMC group, while CD163 and CD206 cells were numerous in other groups (Fig. 6). In the SHM + STLMC group, a significant decrease in the expression of CD163 was detected in the ablated regions and surrounding areas compared with other groups (P<0.05; Fig. 7). The expression of CD206 was also significantly decreased in the SHM + STLMC group compared with other groups (P<0.05; Fig. 7). No significant difference in the expression of

Table III. Number of damaged macrophages observed under light microscopy.

	Day 7					Day 21				
Group	SHM + STLMC	SHM	STLMC	MB	BL	SHM + STLMC	SHM	STLMC	MB	BL
n/HPF	16.86±5.33	5.52±3.00[a]	7.04±3.70[a]	2.12±1.36[a]	0.98±1.00[a]	19.12±4.12[c]	6.50±3.63[b]	5.27±2.71[b]	2.36±1.64[b]	1.22±1.05[b]

Data are presented as the mean ± standard deviation. Comparisons among groups were analyzed using one-way analysis of variance followed by the least significant difference post hoc test. Comparisons between time points were analyzed using Student's t-test. [a]P<0.05 vs. day 7 SHM + STLMC; [b]P<0.05 vs. day 21 SHM + STLMC; [c]P<0.05 vs. day 7 SHM + STLMC. SHM, sub-hyperthermia microwave ablation; STLMC, silibinin-loaded thermosensitive liposome-microbubble complex; MB, microbubble injection; BL, blank control; HPF, high power field.

Figure 6. Immunohistochemical staining for CD163 and CD206 at day 7 after treatment. Cytomembrane positive expression of CD163 was evaluated in the ablated area of the (A) SHM + STLMC, (B) SHM, (C) STLMC and (D) MB groups (scale bar=20 μm; magnification, x400). Cytomembrane positive expression of CD206 was evaluated in the ablated area of the (E) SHM + STLMC, (F) SHM, (G) STLMC and (H) MB groups (scale bar=20 μm; magnification, x400). SHM, sub-hyperthermia microwave ablation; STLMC, silibinin-loaded thermosensitive liposome-microbubble complex; MB, microbubble injection.

CD206 or CD163 was observed between days 7 and 21 in the SHM + STLMC group (P>0.05).

Discussion

Local thermal ablation has become the most widely used method in recent decades because of its technical ease, satisfactory local tumor control and minimally invasive nature (21). However, unfortunately, thermal ablation in HCC treatment is inevitably linked to the development of residual tumors (22). One explanation for this is the heat sink effect, which forms a sub-hyperthermia field at <50˚C. As previous research has demonstrated, considerable heat sink effect is observed within a diameter of 15 mm of simulated vessels, depending on flow rate (23). Therefore, reducing the residual tumors and promoting the long-term efficacy has become a major research focus and various trials have been implemented in the last decade. Feng (24) demonstrated that combining sequential transarterial chemoembolization with radiofrequency ablation (RFA) could obtain a remarkable therapeutic efficacy on HCC. Solazzo *et al* (25) demonstrated that combining RFA

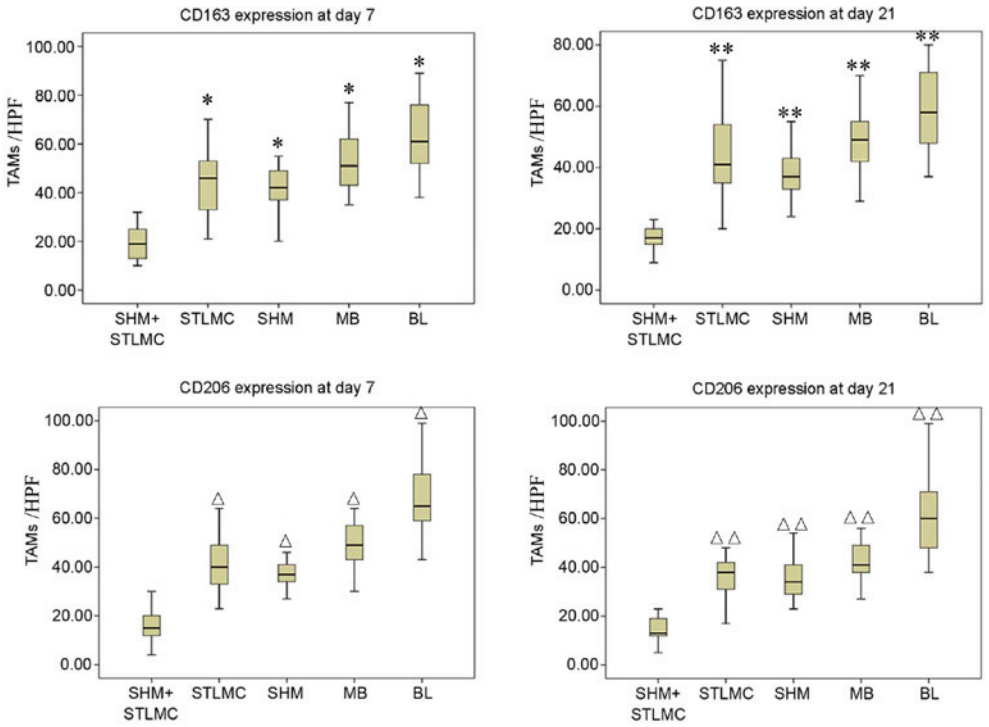

Figure 7. Number of TAMs with CD163 or CD206 positive expression at day 7 or 21 after treatment. *P<0.05 vs. day 7 in the SHM + STLMC group, **P<0.05 vs. day 21 In the SHM + STLMC group; ΔP<0.05 vs. day 7 in the SHM + STLMC group; ΔΔP<0.05 vs. day 21 in the SHM + STLMC group. TAM, tumor-associated macrophage; SHM, sub-hyperthermia microwave ablation; STLMC, silibinin-loaded thermosensitive liposome-microbubble complex; MB, microbubble injection; BL, blank control; HPF, high power field.

with liposomal doxorubicin increases cell injury and apoptosis. A previous study by the present group indicated that combining high-intensity focused ultrasound and injection of microbubbles could expand the effective ablation zone in the treatment of rabbit VX2 liver tumors, thereby decreasing residual tumors (26). In the current study, simulative sub-hyperthermia field was established and an innovative drug carrier, STLMC, was applied to thermal ablation in order to suppress the growth of VX2 tumors and enhance the effect of thermal ablation.

In recent decades, numerous studies have identified that silibinin has anticancer and chemopreventive properties in *in vivo* and *in vitro* cancer models, including lung, brain and kidney cancer (27-30). However, silibinin has poor therapeutic efficacy by oral administration, which may be explained by its poor bioavailability and inadequate water solubility (<0.04 mg/ml), owing to its flavonolignan structure (17). The drug carrier STLMC is composed of microbubbles and liposomes. Microbubbles are destroyed in ultrasound fields and the drugs in the thermosensitive liposome are released in sub-hyperthermia fields. This is considered to enhance the targeting and availability of silibinin (18). In the current study, the tumor volume in the SHM + STLMC group was smaller compared with the other groups at the same time point, which may be due to the effects of silibinin.

By TEM and H&E staining, it was observed in the present study that the number of damaged macrophages increased obviously in the SHM + STLMC group. Meanwhile, numerous inflammatory cells were injured, and apoptotic bodies emerged. This may indicate that the microenvironment was influenced by silibilin being released in sub-hyperthermia fields.

Several previous studies have reported that an increased number of TAMs is closely associated with the angiogenesis, metastasis and poor prognosis of tumors (31-34). Thus, inhibiting TAMs has become a new targeting approach to treat cancers. In the present study, immunohistochemistry results indicated that the cells that expressed CD163 or CD206 in the SHM + STLMC group were obviously decreased compared with other groups. Since TAMS exhibit specific and high expression levels of CD163 and CD206, these results demonstrated that STLMC may control the progress of residual tumors via inhibiting TAMs. Furthermore, under TEM, the macrophages were damaged more seriously on day 21 compared with day 7 in the SHM + STLMC group, and an increased number of damaged macrophages at day 21 SHM + STLMC group was indicated. This may suggest that the inhibitory effect of STLMC on TAMs is enhanced over time.

STLMC could provide a potential method for increasing the efficacy of thermal ablation. However, the mechanisms by which it inhibits TAMs remain unclear. Inflammatory factors, including NF-κB and TGF-β, may serve critical functions in modulating the interactions between TAMs and their surrounding microenvironment (35,36). In the sub-hyperthermia field with STLMC, further research is required to confirm whether the changes observed in TAMs is associated with these inflammatory factors.

For the present study, STLMC was injected within a 10 min period. This administration over a short period may not achieve the satisfactory therapeutic effect. The results of this preliminary study prompt further investigation into the effects of STLMC during ablation, including the local drug concentration and observation of long-term effects.

In summary, when STLMC was involved in the sub-hyperthermia field, a significant decrease in tumor volume accompanied by lower levels of TAMs were observed, which may offer an efficient method to enhance ablation therapy and reduce the occurrence of residual tumors.

Acknowledgements

Sponsorship for the present study and article processing charges was funded by Natural Science Foundation of China (grant no. 81201106).

References

1. Parkin DM, Ferlay J, Curado MP, Bray F, Edwards B, Shin HR and Forman D (eds): Cancer Incidence in Five Continents (CI5) Volumes I to X. IARC CancerBase No. 12. IARC, Lyon, 2014.
2. Ahmed M and Goldberg SN: Basic science research in thermal ablation. Surg Oncol Clin N Am 20: 237-258, vii, 2011.
3. Thanos L, Mylona S, Galani P, Pomoni M, Pomoni A and Koskinas I: Overcoming the heat-sink phenomenon: Successful radiofrequency thermal ablation of liver tumors in contact with blood vessels. Diagn Interv Radiol 14: 51-56, 2008.
4. Vanagas T, Gulbinas A, Pundzius J and Barauskas G: Radiofrequency ablation of liver tumors (II): Clinical application and outcomes. Medicina (Kaunas) 46: 81-88, 2010.
5. Bhardwaj N, Dormer J, Ahmad F, Strickland AD, Gravante G, West K, Dennison AR and Lloyd DM: Microwave ablation of the liver: A description of lesion evolution over time and an investigation of the heat sink effect. Pathology 43: 725-731, 2011.
6. Capece D, Fischietti M, Verzella D, Gaggiano A, Cicciarelli G, Tessitore A, Zazzeroni F and Alesse E: The Inflammatory microenvironment in hepatocellular carcinoma: A pivotal role for tumor-associated macrophages. Biomed Res Int 2013: 187204, 2013.
7. Yang JD, Nakamura I and Roberts LR: The tumor microenvironment in hepatocellular carcinoma: Current status and therapeutic targets. Semin Cancer Biol 21: 35-43, 2011.
8. Solinas G, Germano G, Mantovani A and Allavena P: Tumor-associated macrophages (TAM) as major players of the cancer-related inflammation. J Leukoc Biol 86: 1065-1073, 2009.
9. Sica A and Mantovani A: Macrophage plasticity and polarization: In vivo veritas. J Clin Invest 122: 787-795, 2012.
10. Hao NB, Lü MH, Fan YH, Cao YL, Zhang ZR and Yang SM: Macrophages in tumor microenvironments and the progression of tumors. Clin Dev Immunol 2012: 948098, 2012.
11. Heusinkveld M and van der Burg SH: Identification and manipulation of tumor associated macrophages in human cancers. J Transl Med 9: 216, 2011.
12. Fujiu K, Manabe I and Nagai R: Renal collecting duct epithelial cells regulate inflammation in tubulointerstitial damage in mice. J Clin Invest 121: 3425-3441, 2011.
13. Bosch-Barrera J and Menendez JA: Silibinin and STAT3: A natural way of targeting transcription factors for cancer therapy. Cancer Treat Rev 41: 540-546, 2015.
14. Gu M, Singh RP, Dhanalakshmi S, Agarwal C and Agarwal R: Silibinin inhibits inflammatory and angiogenic attributes in photocarcinogenesis in SKH-1 hairless mice. Cancer Res 67: 3483-3491, 2007.
15. Tyagi A, Singh RP, Ramasamy K, Raina K, Redente EF, Dwyer-Nield LD, Radcliffe RA, Malkinson AM and Agarwal R: Growth inhibition and regression of lung tumors by silibinin: Modulation of angiogenesis by macrophage-associated cytokines and nuclear factor-kappaB and signal transducers and activators of transcription 3. Cancer Prev Res (Phila) 2: 74-83, 2009.
16. Flaig TW, Glodé M, Gustafson D, van Bokhoven A, Tao Y, Wilson S, Su LJ, Li Y, Harrison G, Agarwal R, *et al*: A study of high-dose oral silybin-phytosome followed by prostatectomy in patients with localized prostate cancer. Prostate 70: 848-855, 2010.
17. Cufí S, Bonavia R, Vazquez-Martin A, Corominas-Faja B, Oliveras-Ferraros C, Cuyàs E, Martin-Castillo B, Barrajón-Catalán E, Visa J, Segura-Carretero A, *et al*: Silibinin meglumine, a water-soluble form of milk thistle silymarin, is an orally active anti-cancer agent that impedes the epithelial-to-mesenchymal transition (EMT) in EGFR-mutant non-small-cell lung carcinoma cells. Food Chem Toxicol 60: 360-368, 2013.
18. Duan L, Wen L, Yunfei Z, Jia J, Bangle Z, Guangbin H and Xiaodong Z: Preparation an quality evaluation of sylibinin loaded thermo-sensitive liposome-microbubble complex. Chin J Ulthrasound 31: 250-253, 2015.
19. Liu Y, Yi S, Zhang J, Fang Z, Zhou F, Jia W, Liu Z and Ye G: Effect of microbubble-enhanced ultrasound on prostate permeability: A potential therapeutic method for prostate disease. Urology 81: 921. e1-e7, 2013.
20. Luo W, Zhou X, He G, Li Q, Zheng X, Fan Z, Liu Q, Yu M, Han Z, Zhang J and Qian Y: Ablation of high intensity focused ultrasound combined with SonoVue on rabbit VX2 liver tumors: Assessment with conventional gray-scale US, conventional color/power Doppler US, contrast-enhanced color Doppler US, and contrast-enhanced pulse-inversion harmonic US. Ann Surg Oncol 15: 2943-2953, 2008.
21. Yang PC, Lin BR, Chen YC, Lin YL, Lai HS, Huang KW and Liang JT: Local control by radiofrequency thermal ablation increased overall survival in patients with refractory liver metastases of colorectal cancer. Medicine (Baltimore) 95: e3338, 2016.
22. Feng K and Ma KS: Value of radiofrequency ablation in the treatment of hepatocellular carcinoma. World J Gastroenterol 20: 5987-5998, 2014.
23. Ringe KI, Lutat C, Rieder C, Schenk A, Wacker F and Raatschen HJ: Experimental evaluation of the heat sink effect in hepatic microwave ablation. PLoS One 10: e0134301, 2015.
24. Feng Z: Minshan Chen: Combination of TACE and RFA can improve the treatment of HCC. Ann Transl Med 1: 10, 2013.
25. Solazzo SA, Ahmed M, Schor-Bardach R, Yang W, Girnun GD, Rahmanuddin S, Levchenko T, Signoretti S, Spitz DR, Torchilin V and Goldberg SN: Liposomal doxorubicin increases radiofrequency ablation-induced tumor destruction by increasing cellular oxidative and nitrative stress and accelerating apoptotic pathways. Radiology 255: 62-74, 2010.
26. Luo W, Zhou X, Ren X, Zheng M, Zhang J and He G: Enhancing effects of SonoVue, a microbubble sonographic contrast agent, on high-intensity focused ultrasound ablation in rabbit livers in vivo. J Ultrasound Med 26: 469-476, 2007.
27. Deep G, Gangar SC, Rajamanickam S, Raina K, Gu M, Agarwal C, Oberlies NH and Agarwal R: Angiopreventive efficacy of pure flavonolignans from milk thistle extract against prostate cancer: Targeting VEGF-VEGFR signaling. PLoS One 7: e34630, 2012.
28. Deep G and Agarwal R: Antimetastatic efficacy of silibinin: Molecular mechanisms and therapeutic potential against cancer. Cancer Metastasis Rev 29: 447-463, 2010.
29. Raina K, Agarwal C and Agarwal R: Effect of silibinin in human colorectal cancer cells: Targeting the activation of NF-kB signaling. Mol Carcinog 52: 195-206, 2013.
30. Chang HR, Chen PN, Yang SF, Sun YS, Wu SW, Hung TW, Lian JD, Chu SC and Hsieh YS: Silibinin inhibits the invasion and migration of renal carcinoma 786-O cells in vitro, inhibits the growth of xenografts in vivo and enhances chemosensitivity to 5-fluorouracil and paclitaxel. Mol Carcinog 50: 811-823, 2011.
31. Mantovani A, Sozzani S, Locati M, Allavena P and Sica A: Macrophage polarization: Tumor-associated macrophages as a paradigm for polarized M2 mononuclear phagocytes. Trends Immunol 23: 549-555, 2002.
32. Pollard JW: Tumour-educated macrophages promote tumour progression and metastasis. Nat Rev Cancer 4: 71-78, 2004.
33. Lewis CE and Pollard JW: Distinct role of macrophages in different tumor microenvironments. Cancer Res 66: 605-612, 2006.
34. Bingle L, Brown NJ and Lewis CE: The role of tumour-associated macrophages in tumour progression: Implications for new anticancer therapies. J Pathol 196: 254-265, 2002.
35. Biswas SK, Gangi L, Paul S, Schioppa T, Saccani A, Sironi M, Bottazzi B, Doni A, Vincenzo B, Pasqualini F, *et al*: A distinct and unique transcriptional program expressed by tumor-associated macrophages (defective NF-kappaB and enhanced IRF-3/STAT1activation). Blood 107: 2112-2222, 2006.
36. Benetti A, Berenzi A, Gambarotti M, Garrafa E, Gelati M, Dessy E, Portolani N, Piardi T, Giulini SM, Caruso A, *et al*: Transforming growth factor-beta1 and CD105 promote the migration of hepatocellular carcinoma-derived endothelium. Cancer Res 68: 8626-8634, 2008.

This work is licensed under a Creative Commons Attribution-NonCommercial-NoDerivatives 4.0 International (CC BY-NC-ND 4.0) License.